Journal of Materials Chemistry A

Accepted Manuscript

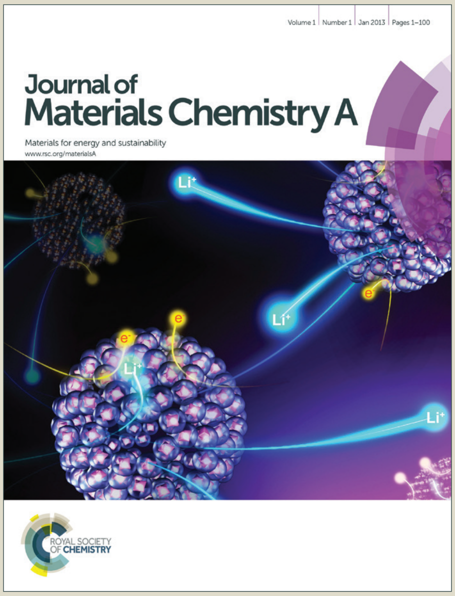

ROYAL SOCIETY OF CHEMISTRY

www.rsc.org/materialsA

Journal of
Materials Chemistry A

RSCPublishing

ARTICLE

Cite this: DOI: 10.1039/x0xx00000x

Received 00th January 2012,
Accepted 00th January 2012

DOI: 10.1039/x0xx00000x

www.rsc.org/

Hierarchical heterostructures of Ag nanoparticles decorated MnO_2 nanowires as promising electrodes for supercapacitors

Hui Xia[a,b*], Caiyun Hong[a,b], Xiaoqin Shi[a], Bo Li[a,b], Guoliang Yuan[a], Qiaofeng Yao[c], Jianping Xie[c,*]

Coating the redox-active transition-metal oxides (e.g., MnO_2) with a conductive metal layer is one efficient approach to improve the electrical conductivity of the oxide-based electrodes, which could largely boost the energy density and power density of supercapacitors. Here, we report a facile yet efficient method to uniformly decorate conductive silver (Ag) nanoparticles (~10 nm) on MnO_2 nanowires (width of ~10-20 nm), which leads to a remarkable improvement of the electrical conductivity and the supercapacitive performance of MnO_2-based electrodes. For instance, at a low scan rate of 10 mV s^{-1}, the as-designed Ag/MnO_2 hybrid electrode delivers a specific capacitance of 293 F g^{-1}, which is twofold higher than that of the bare MnO_2 electrode (~130 F g^{-1}). In addition, the highly conductive Ag nanoparticle layer can also improve the rate capability of the Ag/MnO_2 nanowire electrode, delivering a high specific energy density and power density of 17.8 Wh kg^{-1} and 5000 W kg^{-1}, respectively, at a current density of 10 A g^{-1}.

Introduction

In recent years, supercapacitors have been a topic of strong and sustained interest for the development of next-generation power devices.[1] As one of the energy storage systems, supercapacitors feature with high energy density (better than traditional electrostatic capacitors) and high power density (higher than rechargeable batteries). Due to its high power density, supercapacitors are ideal complementary power devices to rechargeable batteries in applications in diverse fields such as hybrid electric vehicles, mass rapid transit, and power tools. Such power systems typically require high or peak power pulses for a time-dependent usage.[2] In the past few years, the technology of supercapacitors has progressed enormously owing to the development of several new high-performance electrode materials, including the redox-active transition-metal oxides such as RuO_2, NiO, Fe_2O_3, Co_3O_4, SnO_2 and MnO_2. Such oxides are promising as electrode materials due to their high specific capacitances from the fast and reversible redox reactions on the electrode surface.[3-8]

One good example is RuO_2. RuO_2 exhibits good supercapacitive performance due to its large specific capacitance and excellent rate capability. However, the relatively high cost and toxic feature of RuO_2 may severely limit its commercial utility.[9] To address this issue, MnO_2 has been recently surfaced in the community due to its attractive features of high theoretical specific capacitance (~1370 F g^{-1}), good environmental compatibility, and low cost.[10,11] There are several challenges associated with the development of MnO_2-based electrodes. The first one is its relatively small surface area (particularly for the bulk MnO_2), which constrains the energy that could be stored in a MnO_2-based electrode. Scaling down the materials to nanoscale size is a promising solution to address this issue. For example, nanostructured MnO_2 with different morphologies of wires, rods and tubes, have been recently developed and delivered high specific capacitances.[12,13] The second key challenge is the poor electrical conductivity of MnO_2.[14] Its conductivity is in the range of 10^{-6} to 10^{-5} S cm^{-1}; and such poor conductivity may limit the charge-discharge rate of the supercapacitors. To address this issue, combining MnO_2 with some conductive materials such as carbon materials, metals like Au and Ag, and oxides like SnO_2 and Co_3O_4, is very appealing.[15-17]

Among the newly explored conductive materials, Ag is very attractive due to its good conductivity and low cost. Recently, Ag nanoparticles (AgNPs) have been used as conductive dopants in electrode materials for lithium-ion batteries and supercapacitors. For example, AgNPs have been coated on RuO_2, and the resulting Ag-doped RuO_2 exhibited much higher specific capacitance than the pure RuO_2.[17] Similarly, Ag-doped MnO_2 thin films and AgNPs-loaded MnO_2 nanosheets also delivered larger specific capacitances than their bare MnO_2 counterparts.[16,20] Although there are some successful attempts in developing Ag-coated MnO_2-based electrodes, efficient strategies for doping or coating of uniform AgNPs on nanostructured MnO_2 are presently lacking. Here, we report a simple and efficient strategy to fabricate a hierarchical heterostructure of AgNPs-decorated MnO_2 nanowires (or Ag/MnO_2 nanowires). Our strategy is a simple one-pot method to prepare one dimensional hierarchical Ag/MnO_2 nanowires by simply immersing an Ag foil into a mixed solution of $KMnO_4$ and H_2SO_4. The simplicity of the fabrication can be readily transferred to good scalability of our protocol for practical applications. The as-fabricated Ag/MnO_2 nanowires exhibited much larger specific capacitances compared to the bare MnO_2 nanowires with similar size. Furthermore, the Ag/MnO_2 nanowires also showed good rate capability and cycle performance, making them promising electrodes for high-performance supercapacitors.

Experimental

Synthesis of β-MnO_2 nanowires and Ag/MnO_2 composite

The synthesis of AgNPs-decorated MnO_2 nanowires is very simple. In the first step, the Ag foils (99.95% purity, 0.25 mm thickness, Alfa Aesar) were cut into small pieces (2 x 2 cm) and sonicated in acetone, ethanol, and deionized water for 10 min. After that, one piece of Ag foil was immersed into a 100 mL of 0.1 M $KMnO_4$ solution under continuous stirring. Two drops of 98 wt% H_2SO_4 were then introduced into the solution. The reaction mixture with a small piece of Ag foil was continuously stirred at room temperature for 24 h till the solution changed to transparent. The mixed solution was then rested for about one week to obtain the final products. After one week, the precipitates in the solution were collected by centrifugation, followed by washing with copious deionized water. The final products were dried in a vacuum oven at 50 ºC for 12 h. For comparison purpose, β-MnO_2 nanowires were prepared by a similar method as the reported protocol.[21]

Characterization

The microstructure, surface morphology, and chemical composition of the samples were characterized by powder X-ray diffraction (XRD), X-ray photoelectron spectroscopy (XPS), Field emission scanning electron microscopy (FESEM), transmission electron microscopy (TEM), and high resolution transmission electron microscopy (HRTEM). The powder XRD measurements were performed on a Bruker D8 advanced diffractometer with a Cu $K\alpha$ radiation in the 2θ range of 20–80°. XPS spectra were recorded on a Phi Quantera spectrometer using A1 $K\alpha$ X-ray as the excitation source. FESEM and TEM images were taken on a Hitachi S-4800 microscope and a JEOL JEM2100 microscope, respectively, both equipped with EDS. N_2 adsorption-desorption isotherms were measured at the liquid nitrogen temperature using a Micromeritics ASAP 2010 instrument.

Electrochemical measurements

Electrochemical measurements were carried out on the three-electrode cells using a CHI 660D electrochemical workstation. To prepare the working electrode, the active materials (80 wt%, Ag/MnO_2 or MnO_2 nanowires), carbon black (10 wt%) and polyvinylidene difluoride (PVDF, 10 wt%, dissolved in N-methylpyrrolidone (NMP)), were mixed to form a slurry. The slurry was pasted onto a Ti foil and dried for 12 h in a vacuum oven. The loading of the working electrode was typically in the range of ~2-3 mg cm^{-2}. A platinum foil, an Ag/AgCl (saturated KCl) electrode, and a 1.0 M Na_2SO_4 solution, were used as the counter electrode, reference electrode, and electrolyte, respectively. Cyclic voltammetry (CV) and electrochemical impedance spectroscopy (EIS) were used to evaluate the electrochemical behaviors of different composite electrodes. CV measurements were carried out between 0 and 1.0 V (vs. Ag/AgCl) at different scan rates of 10-100 mV s^{-1}. EIS measurements were carried out at a frequency from 10 kHz to 0.01 Hz with an AC amplitude of 10 mV.

Results and discussion

The as-synthesized MnO_2 and Ag/MnO_2 nanowires were first characterized by XRD. As shown in Fig. 1a, all diffraction peaks of MnO_2 nanowires can be indexed to the tetragonal phase of MnO_2 (JCPDS no. 24-0735). No other peaks were observed in the spectrum. As for the XRD spectrum of Ag/MnO_2 nanowires (Fig. 1b), besides the diffraction peaks from the β-MnO_2, four peaks at 38.1, 44.2, 64.5, and 77.4º were observed, which correspond to the (111), (200), (220), and (311) reflections of metallic Ag, respectively (JCPDS no. 65-2871). No phase of silver oxide was observed in the Ag/MnO_2 nanowires. This data provides supportive evidence for the successful synthesis of the AgNPs/MnO_2 nanowires via our simple chemical route.

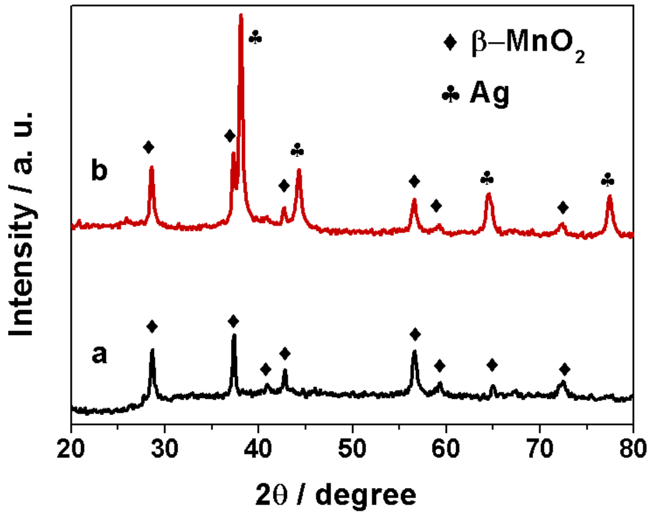

Fig. 1 XRD spectra of (a) the bare MnO_2 nanowires and (b) the Ag/MnO_2 hybrid nanowires.

XPS was used to investigate the oxidation states of the Ag/MnO_2 nanowires. Four elements (Mn, Ag, O, and C) were identified from the full-survey-scan spectrum of the Ag/MnO_2 nanowires (Fig. S1, ESI†). In particular, Fig. 2a shows the Ag 3d core level spectrum, where two distinct peaks at 374.2 and 368.2 eV can be attributed to Ag $3d_{3/2}$ and Ag $3d_{5/2}$, respectively. These values and the 6.0 eV splitting of the 3d doublet signal suggest the presence of metallic Ag, which also agree well with the previous report.[22] As shown in Fig. 2b, two distinct peaks with binding energies of 642.1 and 653.5 eV, and a spin-orbital splitting of 11.4 eV were observed in the Mn 2p core level spectrum. Such values correspond well to the Mn $2p_{3/2}$ and Mn $2p_{1/2}$ in MnO_2.[23] Fig.2c shows the deconvoluted O 1s core-level spectrum, where one sharp peak at 530.1 eV and one small peak at 531.7 eV were observed. The peak at 530.1 eV is a typical state of O^{2-} species in MnO_2, while the small peak could be attributed to the physisorbed, chemisorbed, or dissociated oxygen or hydroxyl species on the surface of the sample, similar to the data reported in a previous study.[24] The XPS spectra, together with the XRD data, strongly support the successful preparation of Ag/MnO_2 composite in our samples.

FESEM and TEM were then used to investigate the morphology of the as-prepared Ag/MnO_2 nanowires. As shown in Fig. 3a, well-dispersed nanowires with high aspect ratios were clearly seen from the FESEM image of the Ag/MnO_2 composite. The nanowires are very thin with a diameter of ~10-20 nm (Fig. 3b). Similarly, the bare β-MnO_2 nanowires synthesized by the hydrothermal method also feature with the same morphology (Fig. S2, ESI†). However, an agglomeration of nanowires was observed in the bare MnO_2 sample, where bundles comprising of several nanowires were clearly seen. Fig. 3b is the representative TEM image of the Ag/MnO_2 nanowires at a low magnification. Some small black dots on the nanowires were observed, and such dots are well-distributed on the surface of nanowires. The high magnification TEM image (Fig. 3c) suggests that the small black dots are monodisperse AgNPs with particle sizes of ~10 nm, and such NPs are closely attached to the surface of MnO_2 nanowires, most likely via the strong bonding between the surface atoms of the AgNPs and the surrounding oxygen of the MnO_2 nanowires. Fig. 3d is a HRTEM image of a single Ag/MnO_2 nanowire, where the lattice fringe with an interplanar spacing of 0.31 nm can be assigned to the (311) planes of β-MnO_2. For the attached AgNPs on the MnO_2 nanowires, an interplanar spacing is determined to be 0.23 (Fig. S3, ESI†), which corresponds well to the (111) planes of the metallic Ag.

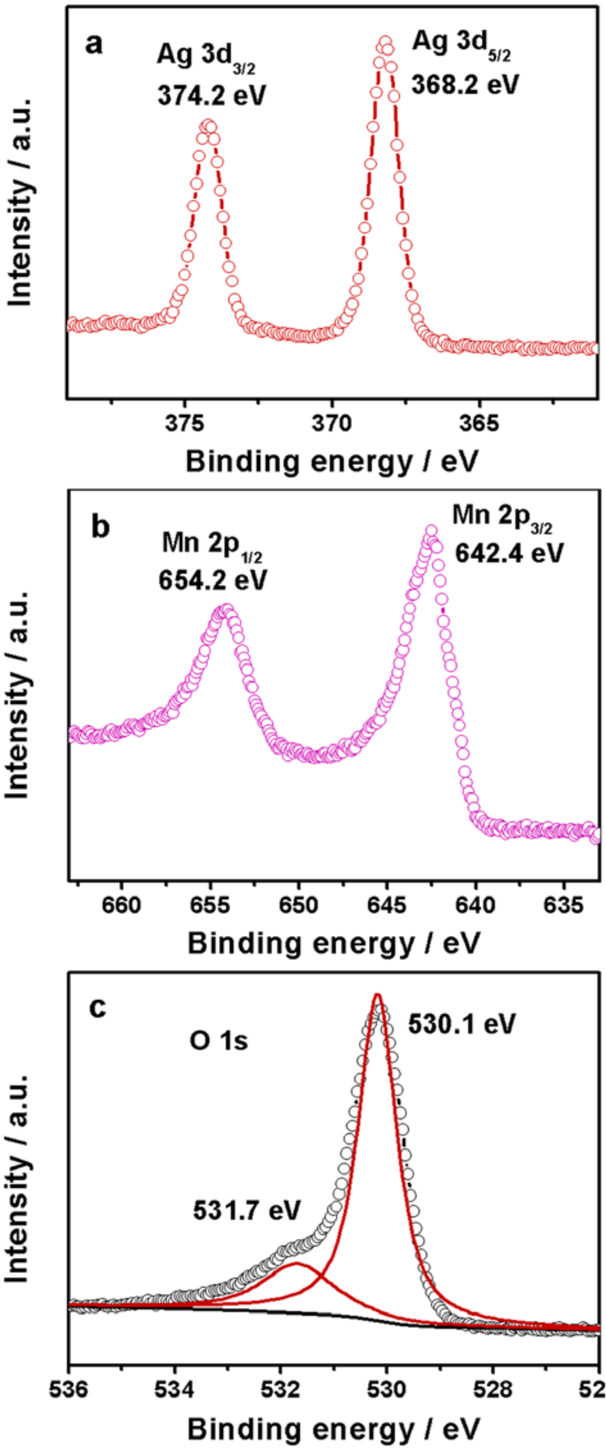

Fig. 2 XPS core-level spectra of (a) Ag 3d, (b) Mn 2p, and (c) O 1s of the as-prepared Ag/MnO_2 hybrid nanowires.

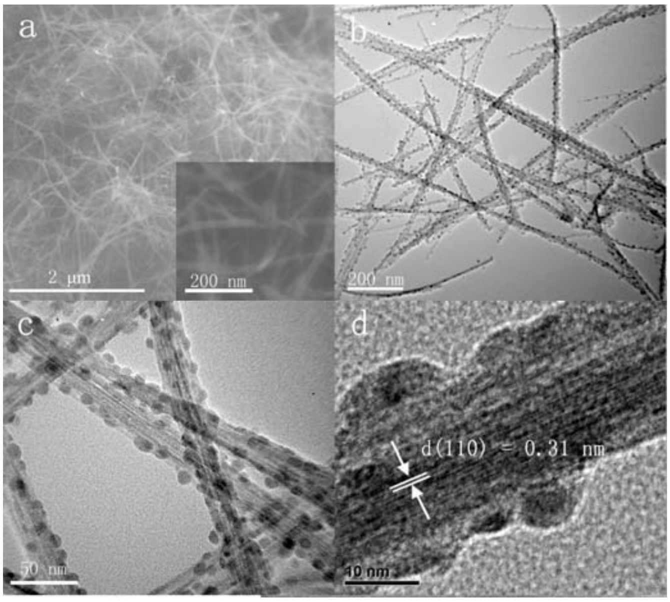

Fig. 3 (a) FESEM image of the Ag/MnO_2 hybrid nanowires. (b) – (d) TEM images of the Ag/MnO_2 hybrid nanowires with different magnifications. Inset in (a) is an enlarged FESEM image of the Ag/MnO_2 hybrid nanowires.

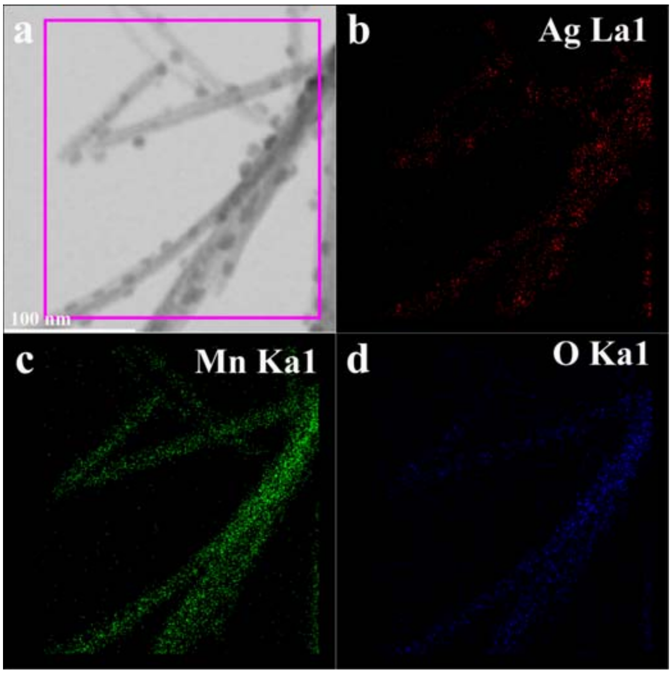

Fig. 4 (a) TEM image of the Ag/MnO_2 hybrid nanowires and EDS element maps of (b) Ag, (c) Mn, and (d) O.

Fig. 4a is a representative TEM image of the Ag/MnO_2 nanowires, with a corresponding energy-dispersive X-ray spectroscopy (EDS) elemental mapping for Ag (Fig. 4b), Mn (Fig. 4c), and O (Fig. 4d). The Mn and O distributions are continuous and well-matched with each other, resembling the morphology of the MnO_2 nanowires. In comparison, the Ag distribution is not continuous, although it also resembles the nanowire morphology, indicating a hierarchical heterostructure of AgNPs well-dispersed on the MnO_2 nanowires. The atomic ratio of Ag to Mn is 1:3, as determined from its EDS spectrum (Fig. S4, ESI†). The EDS line-scanning across one nanowire with two AgNPs (Fig. S5, ESI†) clearly shows that the profile of O overlaps with that of Mn, but not Ag, further suggesting the formation of AgNPs rather than Ag_2O in our composite. The specific surface area of the Ag/MnO_2 hybrid nanowires (~101.8 m^2 g^{-1}) was obtained from analysis of the desorption branch of N_2 gas isotherm (Fig. S6, ESI†).

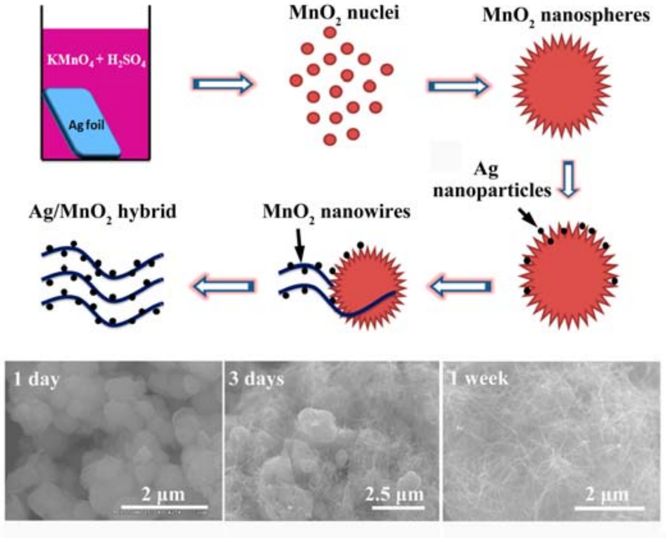

Fig. 5 Schematic illustration of the formation of the hierarchical heterostructures of AgNPs-decorated MnO_2 nanowires.

The chemical route to prepare Ag/MnO_2 nanowires is simple, and it can be schematically illustrated in Fig. 5. When an Ag foil is immersed in the mixed solution of $KMnO_4$ and H_2SO_4, the following reaction (Equation 1) occurs to form MnO_2.

$$2KMnO_4 + 6Ag + 4H_2SO_4 \rightarrow 2MnO_2 + 3Ag_2SO_4 + K_2SO_4 + 4H_2O \qquad (1)$$

$KMnO_4$ is a strong oxidant and it is often used to prepare MnO_2 by reacting with some reducing agents like carbon and Cu.[25] However, without the Ag foil, the mixture of $KMnO_4$ and H_2SO_4 is quite stable at room temperature, and only at an elevated temperature or under a hydrothermal treatment, the $KMnO_4$ in the mixture can be decomposed to form MnO_2.[24] This is distinctively different from the case with a Ag foil, where at the first stage, the chemical reaction between $KMnO_4$ and Ag could generate a large number of MnO_2 nuclei. Such small nuclei possess a large specific surface area and high surface energy, and they intend to aggregate for surface energy reduction. As a result, the concentration of MnO_4^- decreases, and the subsequent growth of the nuclei is restrained due to the exhaustion of the precursors. The aggregated nuclei therefore form spheres consisting of nanosheets, which are formed from the anisotropic growth of MnO_2. However, the as-formed MnO_2 spheres are not very stable in the solution in the presence of Ag^+ ions due to the possible catalytic effect of Ag^+, which was also observed in previous studies.[26,27] Such effects may induce the one-dimensional growth of the as-formed MnO_2 NPs in the reaction solution, leading to the formation of MnO_2 nanowires at room temperature. This process is mild and slow, and it needs about one week to fully convert the MnO_2 spheres to nanowires. In this process, the as-formed Ag_2SO_4 in the solution also gradually decomposes to form AgNPs because of its sensitivity to daylight, according to the following reaction (Equation 2), which is also well-documented.

$$Ag_2SO_4 \rightarrow 2Ag + SO_2 + O_2 \qquad (2)$$

As a result, the decomposition of Ag_2SO_4 leads to the formation of AgNPs, which subsequently attach to the surface of newly-formed MnO_2 nanowires. One week incubation can fully transform the colloidal MnO_2 spheres to the AgNPs-decorated MnO_2 nanowires. In other reports,[28] AgNPs were usually prepared by reduction of $AgNO_3$ using $NaBH_4$. In the present study, the newly developed method can prepare ultrafine AgNPs decorated on MnO_2 nanowires without using such toxic reductant.

The as-fabricated hierarchical heterostructures of AgNPs-decorated MnO_2 nanowires are attractive electrode materials for supercapacitors. We recorded the CV curves of the Ag/MnO_2 and the bare MnO_2 nanowire electrodes at various scan rates from 10 to 100 mV s^{-1}, and with a voltage window of 0-1.0 V (vs. Ag/AgCl in 1.0 M Na_2SO_4 electrolyte). As for the Ag/MnO_2 nanowire electrode (Fig. 6b), all CV curves displayed a quasi-rectangular shape with a perfect mirror-image feature, which suggests an ideal capacitive behavior and good rate capability of the Ag/MnO_2 nanowire electrode. By comparison, the CV curves of the bare MnO_2 nanowire electrode (Fig. 6a) showed a distorted rectangularity, especially for the CV curves at a high scan rate of 100 mV s^{-1}. In addition, the Ag/MnO_2 nanowire electrode delivered a specific capacitance of 293, 261, 226, and 183 F g^{-1} at scan rates of 10, 25, 50, and 100 mV s^{-1}, respectively, while the respective values for the bare MnO_2 nanowire electrode are 130, 95, 72, and 51 F g^{-1} (Fig. 6c). The larger specific capacitance of the Ag/MnO_2 nanowire electrode suggests that the hybrid nanowires can improve the utilization efficacy of MnO_2 for charge storage. In particular, as seen in the FESEM image (Fig. 3a), the Ag-decorated MnO_2 nanowires are well-dispersed, which may provide a large surface area with more active surface sites. In comparison, without the AgNP decoration, the bare MnO_2 nanowires tend to aggregate to form bundles, which may reduce the surface sites of MnO_2 nanowires for charge storage. Moreover, the MnO_2 nanowires prepared in the presence of Ag^+ ions (as a catalyst) at room temperature feature with smaller diameters compared to the MnO_2 nanowires obtained via the hydrothermal method. The smaller size of the Ag/MnO_2 nanowires further increases their surface area. Fig. 6d shows the cycle performance (5000 cycles) of the Ag/MnO_2 and the bare MnO_2 nanowire electrodes at a scan rate of 50 mV s^{-1}. Both samples showed good cycle performance. In particular, after 5000 cycles, the Ag/MnO_2 nanowire electrode still retained ~96.8% of its initial capacitance, slightly higher than that of the bare MnO_2 nanowire electrode (~92.5%).

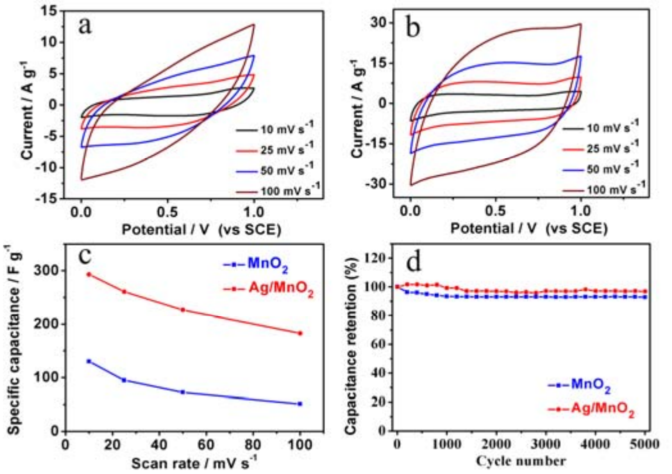

Fig. 6 CV curves of (a) the bare MnO_2 nanowire electrode and (b) the Ag/MnO_2 hybrid nanowire electrode at different scan rates in 1 M Na_2SO_4 electrolyte. (c) Specific capacitances of the Ag/MnO_2 hybrid nanowire (red) and the bare MnO_2 nanowire electrodes (blue). (d) Cycle performance of the Ag/MnO_2 hybrid nanowire (red) and the bare MnO_2 nanowire electrodes (blue) at a scan rate of 50 mV s^{-1} for 5000 cycles.

Fig. 7a and 7b show the galvanostatic charge/discharge curves of the bare MnO_2 nanowire and the Ag/MnO_2 electrodes between 0 and 1.0 V vs. Ag/AgCl in 1.0 M Na_2SO_4 electrolyte, at various current densities from 0.5 to 10 A g^{-1}. A good symmetry and fairly linear slopes were observed in the charge-discharge curves of the Ag/MnO_2 nanowire electrode, indicating a good electrochemical capacitive characteristic and a superior reversible redox reaction. Similar charge/discharge profiles were also observed for the bare MnO_2 nanowire electrode. However, the charge and discharge time for the Ag/MnO_2 nanowire electrode was much longer than that of the bare MnO_2 nanowire electrode at the same current density. This data suggests that the Ag/MnO_2 nanowire electrode has a remarkable improvement in the charge storage capability. The standard electrode potential of Ag^+/Ag is about 0.7996 V, which indicates AgNPs not only improve the electrical conductivity of the hybrid electrode but also contribute to the overall capacitance of the hybrid electrode. In addition, at the current density of 0.5 A g^{-1}, the voltage drop at the beginning of discharge for the Ag/MnO_2 nanowire electrode was much smaller than that of the bare MnO_2 nanowire electrode, which suggests a much smaller internal resistance of the Ag/MnO_2 nanowire electrode. The Ragone plots of the Ag/MnO_2 and the bare MnO_2 nanowire electrodes are presented in Fig. 7c, where the power and energy densities of the hybrid electrode were much larger than those of the bare MnO_2 nanowire electrode. For comparison, the Ragone plots of other recently reported MnO_2-based electrodes have been included in Fig. 7c. It is clear to see that the present Ag/MnO_2 hybrid nanowire electrode exhibits larger or comparable energy and power densities compared to other reported MnO_2-based electrodes.[29-31] In particular, as the current density increased from 0.5 to 10 A g^{-1}, the energy density decreased from 38.1 to 17.8 Wh kg^{-1} for the Ag/MnO_2 nanowire electrode, while the power density increased from 250 to 5000 W kg^{-1}. This data further support the good power capability of the Ag/MnO_2 nanowire electrode. The superior rate capability and power capability of the Ag/MnO_2 nanowire electrode could be attributed to its fast electrode kinetics. For example, Fig. 7d compares the EIS spectra of the Ag/MnO_2 and the bare MnO_2 nanowire electrodes. It is obvious that the Ag/MnO_2 nanowire electrode showed a much smaller charge transfer resistance compared to that of the bare MnO_2 nanowire electrode. Taken together, the large surface area and the improved electrical conductivity of the Ag/MnO_2 nanowire electrode are two key factors for the reduction of its charge-transfer resistance, leading to its superior rate capability and power capability.

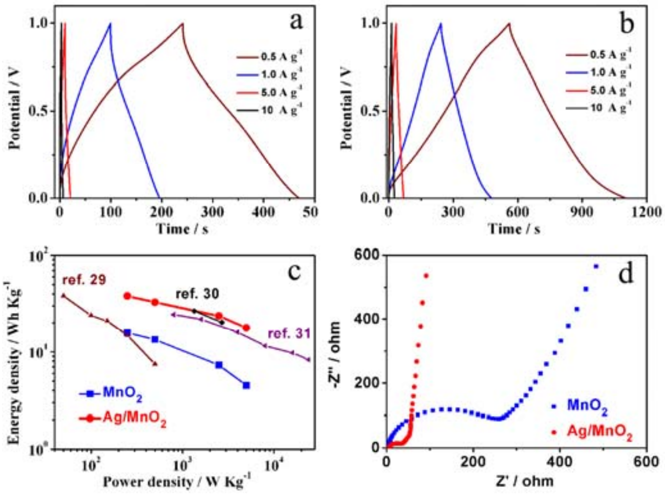

Fig. 7 Charge-discharge curves of (a) the bare MnO_2 nanowire electrode and (b) the Ag/MnO_2 hybrid nanowire electrode at different current densities. (c) Ragone plots of the Ag/MnO_2 hybrid nanowire (red) and the bare MnO_2 nanowire electrodes (blue). (d) Nyquist plots of the Ag/MnO_2 hybrid nanowire (red) and the bare MnO_2 nanowire electrodes (blue).

Conclusions

A hierarchical heterostructure of AgNPs-decorated MnO_2 nanowires was successfully prepared in the present study by using a facile yet efficient chemical protocol. The ultrafine AgNPs with particle sizes of ~10 nm not only suppressed the aggregation of MnO_2 nanowires, but also improved the electrical conductivity of the MnO_2-based electrodes. As a result, the Ag/MnO_2 nanowire electrode showed both improved electrical conductivity and increased surface area, which led to its superior supercapacitive performance, such as large specific capacitance (293 F g^{-1} at a scan rate of 10 mV s^{-1}), good cycle performance (96.8% capacitance retention after 5000 cycles), and excellent rate capability (with a specific energy and power density of 17.8 Wh kg^{-1} and 5000 W kg^{-1} at 10 A g^{-1}, respectively). Such values are better than those of the bare MnO_2 nanowire electrode. The hierarchical heterostructure design presented in this study may provide an efficient platform to improve the electrochemical performance of MnO_2-based electrodes for supercapacitors, and further pave their way towards practical applications.

Acknowledgements

This work was supported by National Natural Science Foundation of China (No. 51102134, 11134004, 51402152), Natural Science Foundation of Jiangsu Province (No. BK20131349), QingLan Project of Jiangsu Province, China Postdoctoral Science Foundation (No. 2013M530258, 2014M551595), and Jiangsu Planned Projects for Postdoctoral Research Funds (No. 1202001B).

Notes and references

[a] School of Materials Science and Engineering, Nanjing University of Science and Technology, Xiaolingwei 200, Nanjing 210094, China E-mail: xiahui@njust.edu.cn .

[b] Herbert Gleiter Institute of Nanoscience, Nanjing University of Science and Technology, Xiaolingwei 200, Nanjing 210094, China.

[c] Department of Chemical & Biomolecular Engineering, Faculty of Engineering, National University of Singapore, Singapore, 117585.E-mail: chexiej@nus.edu.sg

† Footnotes should appear here. These might include comments relevant to but not central to the matter under discussion, limited experimental and spectral data, and crystallographic data.

Electronic Supplementary Information (ESI) available: Full-survey-scan XPS spectrum of MnO_2/Ag hybrid naowires, FESEM image of bare MnO_2 nanowires, high-resolution TEM image of MnO_2/Ag hybrid nanowires, EDS spectrum and EDS line scan spectrum of Ag/MnO_2 nanowires, and N_2 adsorption–desorption isotherms of the Ag/MnO_2 nanowire. See DOI: 10.1039/b000000x/

1 X. H. Lu, M. H. Yu, G. M. Wang and Y. X. Tong, Y. Li, *Energy Environ. Sci.* 2014, **7**, 2160.
2 X. H. Xia, Y. Q. Zhang, D. L. Chao, C. Guan, Y. J. Zhang, L. Li, X. Ge, I. M. Bacho, J. P. Tu and H. J. Fan, *Nanoscale* 2014, **6**, 5008.
3 Y. Wang, C. Y. Foo, T. K. Hoo, M. Ng and J. Y. Lin, *Chem. Eur. J.* 2010, 16, 3598.
4 J. P. Liu, J. Jiang, M. Bosman and H. J. Fan, *J. Mater. Chem.* 2012, **22**, 2419.
5 X. F. Xia, Q. L. Hao, W. Lei, W. J. Wang, D. P. Sun and X. Wang, *J. Mater. Chem.* 2012, **22**, 16844.
6 C. Z. Yuan, L. Yang, L. R. Hou, J. Y. Li, Y. X. Sun, X. G. Zhang, L. F. Shen, X. J. Lu, S. L. Xiong and X. W. Lou, *Adv. Funct. Mater.* 2012, **22**, 2560.
7 W. J. Wang, Q. L. Hao, W. Lei, X. F. Xia and X. Wang, *RSC Adv.* 2012, **2**, 10268.
8 C. Z. Wei, H. Pang, B. Zhang, Q. Y. Lu, S. Liang and F. Gao, *Sci. Rep.* 2013, **3**, 2193.
9 C. C. Hu, K. H. Chang, M. C. Lin and Y. T. Wu, *Nano Lett.* 2006, **6**, 2690.
10 L. Q. Mai, H. Li, Y. L. Zhao, L. Xu, X. Xu, Y. Z. Luo, Z. F. Zhang, W. Ke, C. J. Niu and Q. J. Zhang, *Sci. Rep.* 2013, **3**, 1718.
11 L. Q. Mai, F. Dong, X. Xu, Y. Z. Luo, Q. Y. An, Y. L. Zhao, J. Pan and J. N. Yang, *Nano Lett.* 2013, **13**, 740.
12 W. Xiao, H. Xia, J. Y. H. Fuh and L. Lu, *J. Power Sources* 2009, **193**, 935.
13 H. Xia, J. K. Feng, H. L. Wang, M. O. Lai and L. Lu, *J. Power Sources* 2010, **195**, 4410.
14 H. Pang, S. M. Wang, G. C. Li, Y. H. Ma, J. Li, X. X. Li, L. Zhang, J. S. Zhang and H. H. Zhang, *J. Mater. Chem A* 2013, **1**, 5053.
15 X. H. Lu, T. Zhai, X. H. Zhang, Y. Q. Shen, L. Y. Yuan, B. Hu, L. Gong, J. Chen, Y. H. Gao, J. Zhou, Y. X. Tong and Z. L. Wang, *Adv. Mater.* 2012, **24**, 938.
16 Y. H. Wang and I. Zhitomirsky, *Mater. Lett.* 2011, **65**, 1759.
17 J. Yan, E. Khoo, A. Sumboja and P. S. Lee, *ACS Nano* 2010, **4**, 4247.
18 J. P. Liu, J. Jiang, C. W. Cheng, H. X. Li, J. X. Zhang, H. Gong and H. J. Fan, *Adv. Mater.* 2011, **23**, 2076.
19 H. J. Ahn, Y. E. Sung, W. B. Kim and T. Y. Seong, *Electrochem. Solid-State Lett.* 2008, **11**, A112.
20 G. N. Zhang, L. Zheng, M. Zhang, S. H. Guo, Z. H. Liu, Z. P. Yang and Z. L. Wang, *Energy Fuels* 2012, **26**, 618.
21 F. Zhou, H. G. Zheng, X. M. Zhao, Q. X. Guo, X. M. Ni and T. Shen, *Nanotechnology* 2005, **16**, 2072.
22 P. Gunawan, C. Guan, X. H. Song, Q. Y. Zhang, S. S. J. Leong, C. Y. Tang, Y. Chen, M. B. Chan-Park, M. W. Chang, K. Wang and R. Xu, *ACS Nano* 2011, **5**, 10033.
23 L. Yu, G. Q. Zhang, C. Z. Yuan and X. W. Lou, *Chem. Comm.* 2013, **49**, 137.
24 H. Xia, M. O. Lai and L. Lu, *J. Mater. Chem.* 2010, **20**, 6896.
25 R. J. Fan, Y. Chen, B. Z. Chen and J. W. Wang, *Asia-Pac. J. Chem. Eng.* 2013, **8**, 721.
26 Z. Q. Li, Y. Ding, Y. J. Xiong, Q. Yang and Y. Xie, *Cryt. Growth Des.* 2005, **5**, 1953.
27 Z. Q. Li, Y. Ding, Y. J. Xiong, Q. Yang and Y. Xie, *Chem. Comm.* 2005, **7**, 918.
28 S. Jana, S. Pande, A. K. Sinha, S. Sarkar, M. Pradhan, M. Basu, S. Saha and T. Pal, *J. Phys. Chem. C* 2009, **113**, 1386.
29 Y. S. Luo, J. Jiang, W. W Zhou, H. P. Yang, J. S. Luo, X. Y. Qi, H. Zhang, D. Y. W. Yu, C. M. Li and T. Yu, *J. Mater. Chem.* 2012, **22**, 8634.
30 A. J. Roberts and R. C. T. Slade, *Energ. Environ. Sci.* 2011, **4**, 2813.
31 M. P. Yu, H. T. Sun, X. Sun, F. Y. Lu, G. K. Wang, T. Hu, H. Qiu, J. Lian, *Int. J. Electrochem. Sci.* 2013, **8**, 2313.

Table of contents entry

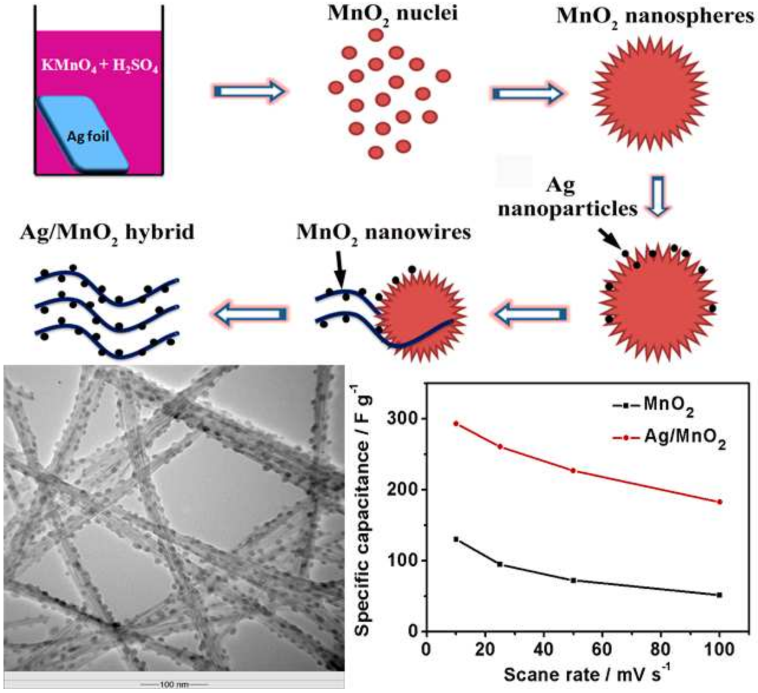

Hierarchical heterostructures of AgNPs-decorated MnO$_2$ nanowires are prepared by a facile yet efficient chemical strategy, and the composite electrode exhibits superior supercapacitive performance compared to the bare MnO$_2$ electrode.